Mechatronic Modeling of a Parallel Kinematics Multi-Axial Simulation Table Based on Decoupling the Actuators and Manipulator Dynamics

Constantino Roldán-Paraponiaris[a,*], Francisco J. Campa[a], Oscar Altuzarra[a]

[a] *Department of Mechanical Engineering, University Of the Basque Country UPV-EHU, C\Alameda Urquijo S/N, Bilbao 48013, Spain*

Abstract

In this work a mechatronic model was developed for a parallel Multi-Axial Simulation Table (MAST) mechanism. The dynamics of the mechanism was obtained using the principle of energy equivalence and Boltzmann-Hamel equations. In this way, the procedure to obtain the explicit dynamic equations is simplified and has the advantage of being systematic. Also, the actuators and the control were modeled and integrated to simulate and study the system's positioning and torque.

A remarkable contribution of this work is that the mechatronic model developed considers the mechanism as a disturbance to the actuators in a decoupled manner, allowing to easily evaluate alternative designs of whether the actuators, the mechanism or both. Additionally, the procedure taken has been validated with experimental data from an actual MAST prototype.

Keywords: Dynamic Modeling, Mechatronic Model, Parallel Mechanisms, Multi-Axial Simulation Table.

1. Introduction

In the last twenty years, parallel kinematics machines have been increasingly used in several fields due to their high performance. For instance, hexapods and tripods are being used for scientific instrumentation due to their high precision positioning in several degrees of freedom[1]. Some solutions present a high stiffness-mass ratio and acceleration which makes them suitable for light machining tasks [2] in an industrial environment. Also, their capability of generating high accelerations makes them interesting for pick & place[3] or for generating harmonically complex motions with great bandwidth, as is the case of excitation tables[4].

Nevertheless, despite their increasing use, they are still complex machines to design, due to their kinematics, dynamics and control. That is why a mechatronic approach with model based design becomes essential for the conception of these machines. For that purpose, complex and detailed simulation tools capable of modeling the manipulator, drives and control dynamics in a cost efficient manner are required.

In that sense, a lot of effort has been putted into modeling the kinematics and dynamics for serial and parallel manipulators. Žlajpah[5] presents an overview of several computational tools (e.g. Matlab/Simulink, Dymola/Modelica) commonly used for simulations purposes focused on robotic systems. As for the dynamics, Lagrange and recursive Newton-Euler methods and the principle of virtual work are commonly employed to obtain the dynamic expressions for serial robotic mechanisms[6]. However, their applicability on parallel manipulators becomes a difficult task because of the kinematic constraints of the closed loops.

Previous works make use of multi-body models of the mechanism [7] or the forward dynamic problem in order to build a mechatronic model. In the first case, it can be justified when high loads are applied to the manipulator, because multibody models are capable of considering the flexible behavior of the machine

*Corresponding author

Email addresses: constantino.roldan@ehu.eus (Constantino Roldán-Paraponiaris), fran.campa@ehu.eus (Francisco J. Campa), oscar.altuzarra@ehu.eus (Oscar Altuzarra)

components. Nevertheless, in that case, expensive software packages may be a limiting factor. On the other hand, with both approaches the contribution of the actuators to the global dynamics is often overlooked, modeling them as a simple inertia and thus assuming a rigid body behavior.

What is more, those formulations can't be used to introduce them in the control algorithm to perform a Compute torque control or a Feed-forward torque control. For that task, the inverse dynamic problem (IDP) has been traditionally used, as it provides the needed torques or forces in the actuators to perform the commanded motion. There are several works where the authors have used this approach to implement control schemes such as model-based control [8, 9]. Codourey [10], developed a model-based control using the IDP to implement a feedforward control for a Delta robot. Similarly, Yang et al. [11] developed a computed force and velocity control for a 6-DOF parallel mechanism also using the inverse dynamics.

Regarding the method to solve the IDP of parallel mechanisms, several formulations have been proposed in the past, as the Newton-Euler[12, 13], the principle of virtual work[14] or Lagrangian methods[15]. Likewise, Lagrangian analysis is frequently employed for open-chains mechanisms. It's use in parallel mechanism yields in very large and often complex set of equations because of the kinematic constraints due to the closed loops of such systems. Also, an interesting approach with Newton-Euler has been taken in [13], where intermediate variables from the joint-space and matrix algebraic manipulation tools are used to obtain explicit dynamic models for a Gough-Stewart platform . In general, their applicability on parallel mechanisms is difficult due to the kinematic constraints caused by the closed loops [16]. As an alternative, with other methods of analytical mechanics (i.e. Boltzmann-Hamel equations, quasi-velocities and principle of energy equivalence[17]), the difficulty in finding a dynamic model suitable for computer simulations is greatly reduced.

Moreover, the common approach is to focus on the manipulator and then include the actuators. However, in several applications, especially when the payload and the manipulator are relatively light, the control cycle time or even the actuators dynamics can be more restrictive due to their finite stiffness, which limits the bandwidth and thus the dynamic performance of the machine in terms of speed, acceleration and trajectory tracking [18, 19, 20].

In the present work, a procedure for the mechatronic modeling of parallel kinematics machines is proposed, taking into account the rigid body dynamics of the manipulator, the compliant dynamics of the actuators and the cycle time of the control loops. The method is based on decoupling the dynamics of the actuators from the manipulator, in such a way that forces needed to move the manipulator are considered as a disturbance from the point of view of the actuators. This scope allows modeling the manipulator dynamics using the inverse dynamic problem, relating the motion of the actuators with the forces that generate the motion of the manipulator. To do so, although any method can be used, here it is proposed to use the Principle of energy equivalence and the Boltzmann-Hamel equations to compute the IDP. The actuators modeling and their transmission chain can be performed with great detail using a model of several degrees of freedom affected by the disturbance forces from the mechanism and the friction. Finally, the cycle time of the position, velocity and current control loops is taken into account. The whole model has been programmed in Matlab Simulink.

There are several advantages for this procedure. First, it is easy to evaluate alternative designs. Given the fact that models of control, actuators and manipulator are decoupled and represented by blocks, it is possible to replace them with new blocks representing alternative configurations. This reduces the time and effort required in the design and simulation stage for a given application yet being reliable. Second, it is possible to better evaluate the interaction between control, actuators and mechanism. For example, the bandwidth of the actuators alone vs. the bandwidth of the whole manipulator can be analyzed. Also, it is possible to isolate and evaluate the influence of the dynamic parameters of the manipulator or the actuator transmission chain on the tracking error. Simulation of the cycle time and its effect on the trajectory tracking and the driving forces allows also a better definition of the control specifications of the final prototype. Third, the use of the inverse dynamic problem results in an explicit set of equations that allows a fast computation comparing with multibody techniques and can be used also to improve the control algorithm if needed. Fourth, the use of the Principle of energy equivalence and the Boltzmann-Hamel equations allows for a more systematic and error free computation of the IDP for parallel mechanisms.

This article is organized as follows. First, in section 2, the proposed procedure for mechatronic modeling

of parallel kinematic machines will be detailed. Second, in section 3, a case study based on a 3PRS mechanism will be given where the aforementioned procedures are employed. Third, the results of an experimental validation will be commented in section 4. Finally, the main conclusions are presented.

2. Mechatronic modeling for parallel kinematic mechanisms

The method here proposed for the mechatronic modeling of parallel manipulators considers the actuators and the manipulator as two independent subsystems whose interaction is due to the Newton's third law. That is, from the actuators viewpoint, the mechanism generates some forces that work as a disturbance against their motion but, at the same time, those forces are the input that provides the manipulator's motion. That interaction is represented by F_i forces in Fig. 1 in a generic parallel manipulator. The result is that the actuators, which often times limit the overall system's performance, can be modeled in a more detailed fashion. On the other hand, to include the influence of the mechanism in the mechatronic model, the inverse dynamic problem (IDP) is solved, with the advantage that those equations can also be used in the control algorithm. Also, the control algorithm as in Fig. 2 and the cycle time of the closed loops has been considered due to their impact on the trajectory tracking, bandwidth and disturbance rejection. To the best of the authors knowledge, this approach that considers the mechanism as a disturbance for the actuators allows a deeper analysis of the interaction between control, actuators and mechanism and has not been addressed before.

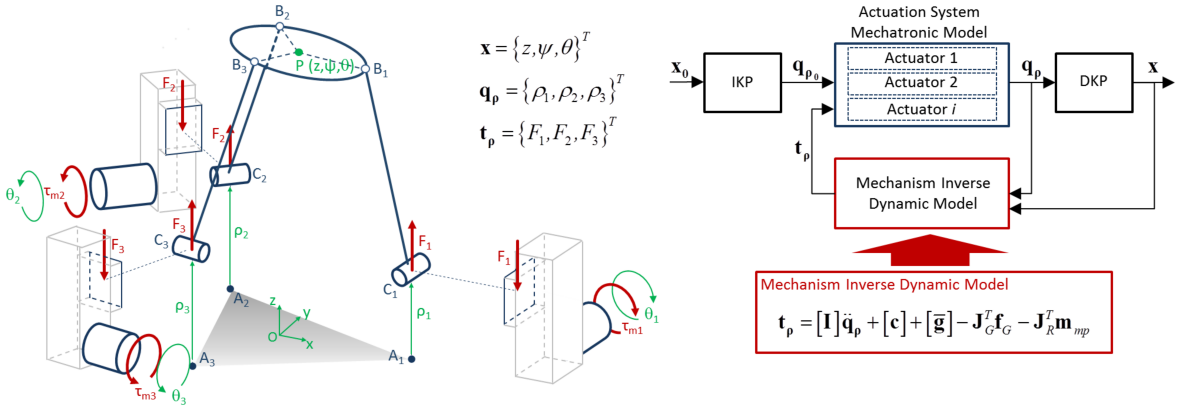

Figure 1: Mechatronic model of a parallel kinematics machine with joint sace position control: manipulator position in workspace ($\mathbf{x}$), manipulator position in joint space (ρ), actuators position at the motor encoders ($\theta_\mathbf{i}$), reactions between the manipulator and actuators (τ), motor torques ($\tau_\mathbf{mi}$).

2.1. Mechatronic model of the manipulator

In Fig. 1 a mechatronic model of a manipulator is shown. It is assumed a joint space position control, where the control reacts to the position error measured in the actuated joints ρ. This decision was taken since it is widely found in general industrial applications. However, more complex control algorithm can also be employed as will be shown in section 2.3. In this way, the end platform position commands $\mathbf{x_0}$ are converted to the joint space through the inverse kinematic problem. Those $\mathbf{q}_{\rho_0}$ commands are then introduced into the mechatronic model of the actuators. As a result, the actuators reach a position $\mathbf{q}_\rho$ and the end platform location $\mathbf{x}$ is calculated with the direct kinematic problem. A rigid body behavior is here considered for the mechanism. To model the influence of the mechanism dynamics on the global behavior, the forces $\mathbf{t_p}$ generated to perform the motion are calculated with the IDP once actuators and platform motion are known. Those forces are then introduced as a disturbance into the actuators mechatronic model, in which a cascaded control in position, velocity and current is assumed. There, the mechanism forces are converted into a torque disturbance on the motor, thus acting as an opposition to the actuator.

2.2. Mechatronic model of the actuators

Regarding the actuator control model, a proportional position control with gain k_v is considered. If two encoders are used, a rotary one for the motor and a linear one for the actuator table, it is possible to control directly the linear position ρ. The velocity and current control loops in Fig. 2 are based on a PI control, where k_p, k_i, k_{pc} and k_{ic} are the proportional and integral gains, respectively for each loop. Furthermore, their cycle times can be taken into account, sampling the signals and using the z-domain for the transfer functions of the system. Also, the response of the electrical part is modeled by taking into account the resistance R and inductance L of the circuit in $TF_{electric}$, as well as the torque constant k_T and the counter electromotive constant k_E.

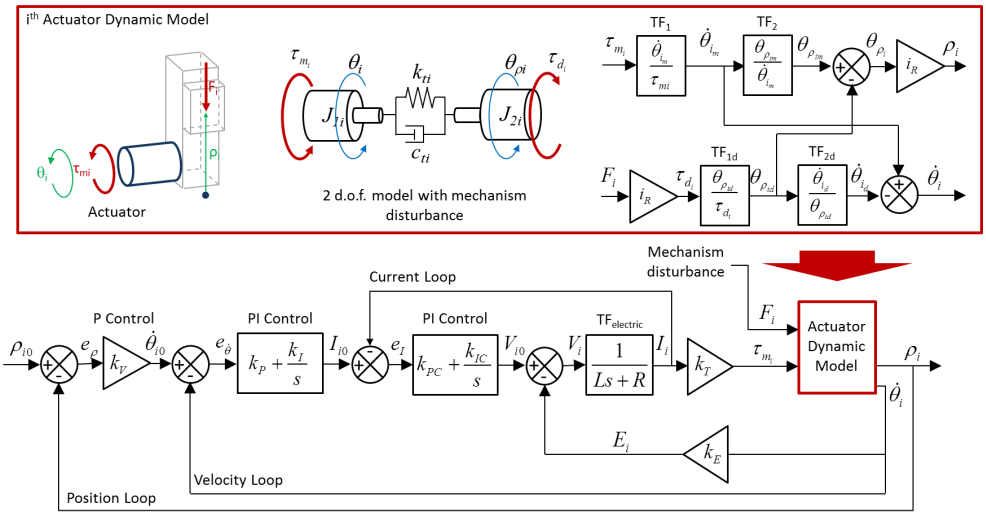

Figure 2: $\mathbf{i^{th}}$ actuator mechatronic model.

With respect to the mechanical behavior of the actuators, the two degrees of freedom model as shown in Fig. 2 has been used, where the motor torque τ_m and the disturbance force F are the inputs. The latter is converted to a torque disturbance applied to the motor by means of equation 1, where p is the pitch of the linear guide and i_r is the gear ratio of the gearbox. Likewise, the outputs are the linear position of the guide ρ, whose angular equivalent is θ_ρ, and the motor's angular velocity $\dot{\theta}$. Furthermore, the actual angular position of the guide is obtained from the ideal position θ_{ρ_m} and the position variation due to the disturbance θ_{ρ_d}. Similarly, the actual velocity is obtained from the motor's ideal velocity $\dot{\theta}_m$ and the velocity variation $\dot{\theta}_d$ also caused by the disturbance.

The aforementioned magnitudes are related by four transfer functions (TF). The first, TF_1 in Eq. 2, relates the angular position of the motor without disturbance θ_m and the input torque τ_m. The actuator's flexible dynamics are represented by the damping C_t and stiffness K_t. Moreover, the inertia of the driving part is represented by J_1 whereas J_2 represents the inertia of the transmission. The second transfer function, TF_2 also in Eq. 2, relates the equivalent ideal angular position of the linear guide θ_{ρ_m} with the motor's position θ_m. The remaining transfer functions are employed to model the disturbances. On one hand, TF_{1d} in Eq. 3 relates the disturbance torque τ_d with the angular equivalent of the position disturbance in the linear guide θ_{ρ_d}. On the other hand, TF_{2d} (see Eq. 3) relates θ_{ρ_d} with the position variation at the motor's shaft due to the disturbance θ_d. It should be noted that these transfer functions must be derived to match the magnitudes when appropriate. Finally, depending on the transmission complexity and stiffness, they can be obtained from a one, two, or N degrees of freedom model. The one DoF model is suitable for actuators that could be considered as stiff or that operate in a relatively low frequency range. Otherwise, a N DoF model is required if the damping and flexibility of its components is not negligible.

$$i_R = \frac{p}{2\pi i_r} \tag{1}$$

$$TF_1 = \frac{\theta_m}{\tau_m} = \frac{J_2 s^2 + c_t s + k_t}{s^2 \left(J_1 J_2 s^2 + (J_1 + J_2)\, c_t s + (J_1 + J_2)\, k_t\right)} \qquad TF_2 = \frac{\theta_{\rho_m}}{\theta_m} = \frac{c_t s + k_t}{(J_2 s^2 + c_t s + k_t)} \tag{2}$$

$$TF_{1d} = \frac{\theta_{\rho_d}}{\tau_d} = \frac{J_1 s^2 + c_t s + k_t}{s^2 \left(J_1 J_2 s^2 + (J_1 + J_2)\, c_t s + (J_1 + J_2)\, k_t\right)} \qquad TF_{2d} = \frac{\theta_d}{\theta_{\rho_d}} = \frac{c_t s + k_t}{(J_1 s^2 + c_t s + k_t)} \tag{3}$$

2.3. Control alternatives

~~Although in Fig. 1 the approach here proposed is applied to a joint space control, it is possible to consider other control strategies~~. The main problem of the joint space control is that it reacts against the position error measured in the actuated joints of the manipulator, so every error in the kinematic chain of the mechanism is not considered. Nevertheless, it is a convenient alternative due to the generally difficult access to a direct measurement of the end platform in parallel kinematic machines.

As opposed to joint-space control schemes, workspace control reacts to the position error $\mathbf{e}_x$ measured directly in the end platform. This alternative can be modeled as it is shown in Fig. 3a and compared to the joint space alternative. In this case, the position control is performed in the manipulator level and not in the actuator model. As such and upon receiving a workspace position $\mathbf{X_0}$, the error is calculated with the actual position $\mathbf{X}$ which is then passed through the gain $\mathbf{k}_v$. A velocity command $\dot{\mathbf{X}}_\mathbf{0}$ results and is converted to the actuated joints coordinates $\dot{\mathbf{q}}_{\rho_0}$ by using the inverse kinematic problem (IKP). At the same time, the disturbance $\mathbf{t}\rho$ is calculated and fed into the actuators models along with the joint coordinates. Finally the actual joints positions are obtained and passed through the direct kinematic problem (DKP) to obtain the actual workspace positions $\mathbf{X}$. Other control algorithms, such as ~~Computed Torque Control~~

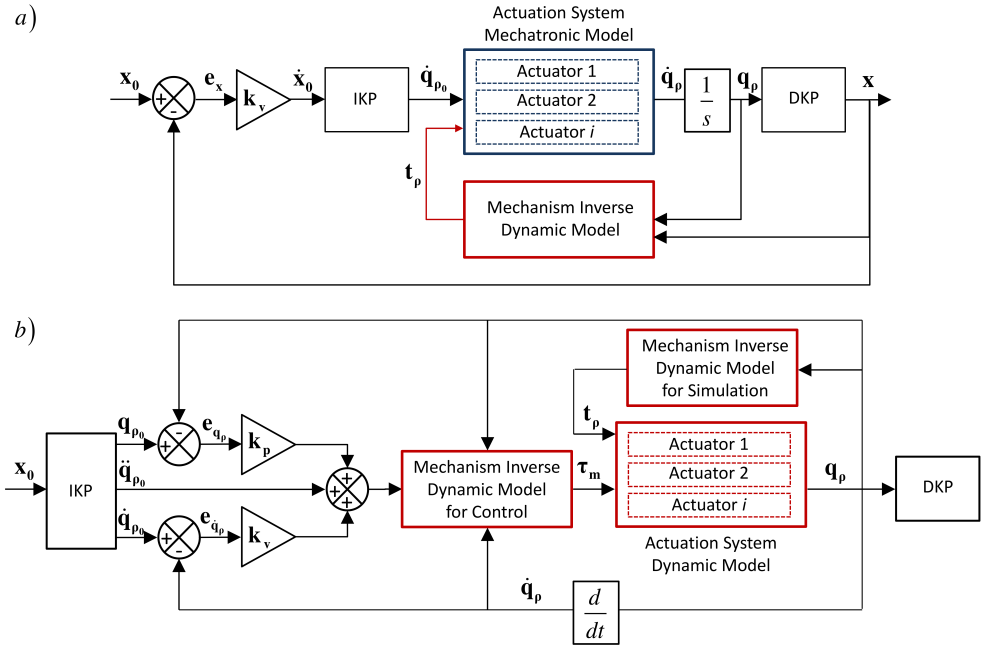

Figure 3: Mechatronic model for: a) Workspace Position Control.b) Computed Torque Control.

~~and estimators-based controllers~~ estimators-based controllers or *computed torque control*(CTC) can also be employed [21] and [22]. As an example, a simple scheme for the CTC case is shown in figure 3b. First, the command $\mathbf{X_0}$ is converted to position ($\mathbf{q}_{\rho_0}$), velocity ($\dot{\mathbf{q}}_{\rho_0}$) and acceleration ($\ddot{\mathbf{q}}_{\rho_0}$) at the joints with the IKP. Then, the position and velocity errors ($\mathbf{e}_{q_\rho}$, $\mathbf{e}_{\dot{q}_\rho}$) are computed and passed through the position and velocity gains ($\mathbf{k_p}$, $\mathbf{k_v}$) respectively and added to $\ddot{\mathbf{q}}_{\rho_0}$. Afterwards, the acceleration signal is used in

the inverse dynamic model (IDP) of the mechanism to obtain the required torques τ_m for the actuators. Also, the disturbance $\mathbf{t}_\rho$ are calculated and introduced to the actuators's models where the actual positions, velocities and accelerations in $\mathbf{q}_\rho$ are obtained. Finally, these are then used in the DKP to calculate the workspace position of the mechanism.

2.4. Inverse dynamic problem modeling

For simulation and control purposes, differential equations in terms of the actuation geometrical kinematic variables, mass properties and applied forces by the actuators are required. This form of dynamic problem results in inertial $\mathbf{I}_G$, gravitational $\bar{\mathbf{g}}_G$ and Coriolis $\mathbf{c}_G$ terms obtained separately.

With the input variables of the mechanism defined as $\mathbf{q}_\rho$, each link can be expressed with the Lagrange function $\mathcal{L}_{mech}$ (Eq. 4) in terms of these input variables to apply the Euler operator $\mathcal{E}_{\mathbf{q}_\rho}$ [17].

$$\mathcal{E}_{\mathbf{q}_\rho}\left(\mathcal{L}_{mech}\right) = \frac{d}{dt}\frac{\partial \mathcal{L}_{mech}}{\partial \dot{\mathbf{q}}_\rho} - \frac{\partial \mathcal{L}_{mech}}{\partial \mathbf{q}_\rho} = \mathbf{f}_\rho = \mathbf{t}_\rho + \mathbf{Q}_\rho \tag{4}$$

In this equation, $\mathbf{f}_\rho$ is the generalized forces vector which include input torques $\mathbf{t}_\rho$ in terms of the input variables $\mathbf{q}_\rho$, and $\mathbf{Q}_\rho$ represents the generalized output forces. This equation will be used to simulate the torque depending on the kinematic variables of the actuators. In the case of parallel mechanism, obtaining such equation is a difficult task due to the constraints of closed-chains kinematics[15]. By using dependent coordinates this problem can be simplified. Basically, the mechanism can be separated and each of its subsystem can be analyzed independently, as long as the motion conditions are the same as the assembled system. This approach has been followed before in [23] and [24] using Lagrange multipliers $\lambda's$ which have also to be calculated. An alternative is to employ the principle of energy equivalence [15].

Essentially, it states that the sum of each subsystem's energy is the same as the assembled system energy. This avoids the additional calculus of the Lagrange multipliers. However, in spatial rotation such as in the case of the end effector, the kinetic energy results in multiplication of angular derivatives terms by trigonometric functions, which yields in a complex expression of $\mathcal{L}_{mech}$. To avoid this, quasi-velocities can be used as generalized coordinates requiring to employ Boltzmann-Hamel equations instead of the Euler operator.

2.4.1. Principle of energy equivalence applied to planar motion

The mechanism is separated into N free-body subsystems each one represented by its generalized coordinates q_{bi} and grouped into the set ~~q_b~~ $\mathbf{q}_b$. To maintain the energy equivalence with the original system, all subsystems have to move as if they were assembled. This condition implies that ~~q_b~~ $\mathbf{q}_b$is a function of the generalized coordinates of the assembled mechanism $\mathbf{q}_\rho$. ~~Thus, the virtual displacements are related as in Eq. 5.~~ Thus, the virtual displacements $\delta\mathbf{q}_b$ for all subsystems are related with the Jacobians to the virtual displacement $\delta\mathbf{q}_\rho$ of the generalized coordinates as shown in Eq. 5.

$$\delta\mathbf{q}_b = \frac{\partial \mathbf{q}_b}{\partial \mathbf{q}_\rho}\,\delta\mathbf{q}_\rho = \mathbf{J}\,\delta\mathbf{q}_\rho; \qquad \delta\mathbf{q}_{b_i} = \mathbf{J}_{b_i}\,\delta\mathbf{q}_\rho \qquad i = 1\ldots N \tag{5}$$

In this equation, $\mathbf{J}$ and $\mathbf{J}_{b_i}$ are the Jacobians for the assembled and for each subsystem respectively, which were obtained from the kinematic problem. They relate the generalized coordinates of each subsystem $\mathbf{q}_{b_i}$ with the ones of the assembled mechanism $\mathbf{q}_\rho$. Also, the energy equivalence implies that, the virtual work of the assembly δW_ρ is equal to the sum of the virtual work of all subsystems $\sum_{i=1}^{N}\delta W_{b_i}$. ~~This relation is represented by the virtual work of Eq. 6.~~ This relation is presented in detail in Eq. 6.

$$\delta W_\rho = \delta\mathbf{q}_\rho^T\mathbf{f}_\rho = \delta W_b = \sum_{i=1}^{N}\delta W_{b_i} = \sum_{i=1}^{N}\delta\mathbf{q}_{b_i}^T\mathbf{f}_{b_i} \tag{6}$$

Furthermore, by substituting Eq. 6 into Eq. 5, the forces due to the manipulator's bars $\mathbf{f}_\rho$are obtained.

$$\mathbf{f}_\rho = \mathbf{J}^T\mathbf{f}_b = \sum_{i=1}^{N}\mathbf{J}_{b_i}^T\mathbf{f}_{b_i} \tag{7}$$

Finally, when each subsystem is disassembled, ~~the~~joint forces between solidsarise which also produce virtual work. However, when the contributions $\mathbf{J}_{b_i}^T \mathbf{f}_{b_i}$ of ~~all~~ eachsubsystem ~~s~~are summed up like in Eq. 7, that virtual work gets canceled by the corresponding reaction of the adjacent subsystem, thus it is unnecessary to take them into account.

2.4.2. Boltzmann-Hamel equations applied for spatial rotation

The end-effector of the 3PRS mechanism herein considered is capable of constrained translation and rotation motions. Decoupling both motions, the dynamics can be studied more effectively. Regarding the contribution of the platform translation to the global dynamics, by considering the coordinates of the center of mass as generalized coordinates $\mathbf{q}_G = [x_G,\ y_G,\ z_G]^T$, an applied external force at that point $\mathbf{f}_G$, and the kinematic relationship with the input variables through the corresponding Jacobian $\mathbf{J}_G$, equations 8 and 9 are obtained, where $\mathbf{M}_G$ is the mass matrix and $\mathbf{I}_G$, $\bar{\mathbf{g}}_G$ and $\mathbf{c}_G$ are recalled to be the inertial, gravitational and Coriolis terms matrices.

$$\mathbf{J}_G^T \mathbf{f}_G = \mathbf{J}_G^T \mathbf{M}_G \mathbf{J}_G \ddot{\mathbf{q}}_\rho + \mathbf{J}_G^T \mathbf{M}_G \dot{\mathbf{J}}_G \dot{\mathbf{q}}_\rho + \mathbf{J}_G^T \mathbf{g}_G \tag{8}$$

$$\mathbf{J}_G^T \mathbf{f}_G = \mathbf{I}_G \ddot{\mathbf{q}}_\rho + \mathbf{c}_G + \bar{\mathbf{g}}_G \tag{9}$$

However, when trying to obtain an expression of the rotation kinetic energy, complex terms of trigonometric functions multiplying angular derivatives arises as a result of the spatial rotation of the element. This yield in a effort when trying to obtain the expressions of the dynamics. By using quasi-velocities as the generalized coordinates, as opposed to position coordinates, the problem can be simplified. Nevertheless, this would imply that Boltzmann-Hamel equations have to be used instead of Euler's operator.

In this work, Boltzmann-Hamel equations are applied to obtain the pure rotation dynamics of the final platform. For this, the angular velocities $\mathbf{w}$ with respect to a reference system attached to the mobile platform, and the Euler's angle ~~$\mathbf{q}$~~ $\mathbf{q}_e$, are expressed as in equations 10 and 11.

$$\mathbf{w} = [\omega_x, \omega_y, \omega_z]^T \tag{10}$$

$$\text{~~}\mathbf{q} =\text{~~}\mathbf{q}_e = [\theta_e, \psi_e, \phi_e]^T \tag{11}$$

Furthermore, the relationship between $\mathbf{w}$ and $\dot{\mathbf{q}}_e$can be written as ~~follows~~ in Eq. 12, where ${\mathbf{D}_\phi}^T$ is the projection matrix between both vectors. It is important to stress that matrix ${\mathbf{D}_\phi}^T$ may be rank deficient depending on the orientation of the rigid body relative to the defined coordinate system. Such a problem is commonly found with every parametrization of the orientation and is specially present in the case of large rotation angles ($\geqslant 180$). Nevertheless, rank deficiency can be avoided by properly choosing an orientation of the coordinate system that ensures that the singularities are beyond the actual orientation workspace. This guarantees a full rank matrix and hence good numerical results. Another approach is to employ *quaternions* to express the rotation of the platform. Yet, this would result in unnecessary more complex dynamic equations for the mechanism herein studied since the maximum permitted angle of motion is defined to be 20°.

$$\mathbf{w}\left(\dot{\mathbf{q}}_e, \mathbf{q}_e\right) = {\mathbf{D}_\phi}^T \dot{\mathbf{q}}_e = \begin{bmatrix} \cos\phi_e & \sin\theta_e \sin\phi_e & 0 \\ -\sin\phi_e & \sin\theta_e \cos\phi_e & 0 \\ 0 & \cos\theta_e & 1 \end{bmatrix} \begin{Bmatrix} \dot{\theta}_e \\ \dot{\psi}_e \\ \dot{\phi}_e \end{Bmatrix} \tag{12}$$

As a result of applying the Boltzmann-Hamel equations as described in [15] [16], the moment due to the rotation of the platform $\mathbf{m}_{mp}$is obtained as in Eq. 13. In this equation, $\mathbf{I}_{mp}$ is the inertia matrix with respect of a coordinate system fixed to the platform.

$$\mathbf{m}_{mp} = \mathbf{I}_{mp} \dot{\mathbf{w}} + \mathbf{w} \times (\mathbf{I}_{mp} \mathbf{w}) \tag{13}$$

Furthermore, on account of considering the mechanism as a disturbance to the actuators, this moment has to be expressed with respect to the input variables. Hence, the Jacobian matrix $\mathbf{J}_\mathbf{R}$, which relates

the inputs in $\mathbf{q}_\rho$ and the velocities $\mathbf{w}$, is used to *project* the rotation dynamics onto the actuation system. Therefore, Eq. 13 is operated and rewritten as follows.

$$\mathbf{J}_R^T \mathbf{m}_{mp} = \mathbf{J_R}^T \left[\mathbf{D}_\phi \mathbf{I}_{mp} \dot{\mathbf{w}} + 2\dot{\mathbf{D}}_\phi \mathbf{I}_{mp} \mathbf{w} - \mathbf{A}^T \mathbf{I}_{mp} \mathbf{w} \right] \tag{14}$$

Where

$$\mathbf{A} = \left(\frac{\partial \dot{\mathbf{w}}}{\partial \dot{\mathbf{q}}_e} \right) \tag{15}$$

The time derivatives of $\mathbf{w}$ and $\dot{\mathbf{q}}_e$ are defined as

$$\dot{\mathbf{w}} = \dot{\mathbf{D}}_\phi^T \dot{\mathbf{q}}_e + \mathbf{D}_\phi^T \ddot{\mathbf{q}}_e \tag{16}$$

$$\ddot{\mathbf{q}}_e = \mathbf{J} \ddot{\mathbf{q}}_\rho + \dot{\mathbf{J}} \dot{\mathbf{q}}_\rho \tag{17}$$

Finally, by substituting when appropriate into Eq. 14, the expression representing the rotation dynamics is found separated by the inertial term $\bar{\mathbf{I}}_{mp}$ and the quadratic velocity term $\mathbf{c}_{mp}$.

$$\mathbf{J}_R^T \mathbf{m}_{mp} = \mathbf{J}_R^T \mathbf{I}_{mp} \mathbf{J}_R \ddot{\mathbf{q}}_\rho + \mathbf{c}_{mp} = \bar{\mathbf{I}}_{mp} \ddot{\mathbf{q}}_\rho + \mathbf{c}_{mp} \tag{18}$$

Where,

$$\mathbf{c}_{mp} = \left[\mathbf{J}^T \left[\mathbf{D}_\phi \mathbf{I}_{mp} {\mathbf{D}_\phi}^T \right] \dot{\mathbf{J}} + \mathbf{J}^T \left[\mathbf{D}_\phi \mathbf{I}_{mp} \dot{\mathbf{D}}_\phi^T + 2\dot{\mathbf{D}}_\phi \mathbf{I}_{mp} {\mathbf{D}_\phi}^T - \mathbf{A}^T \mathbf{I}_{mp} {\mathbf{D}_\phi}^T \right] \mathbf{J} \right] \dot{\mathbf{q}}_\rho \tag{19}$$

It is important to note that equations 18 and 19 do not lack of generality and thus can be used for any manipulator, provided that $\mathbf{I}_{mp}$ and $\mathbf{J_R}$ are appropriately modified. As a contribution, the proposed procedure has the advantage of being systematic, which is less error prone than when trying to obtain particular dynamic equations for a given mechanism.

3. Case study

The case study is based on an actual 3PRS Multi-Axial Simulation Table (MAST) parallel mechanism. A picture of the prototype used is shown in Fig. 4. Moreover, the important geometric variables are also shown in Fig. 4. The dimensions of the actual mechanism are $r = 0.35[m]$, $L = 0.26[m]$ and $H = 0.4[m]$. The mass of the legs is $0.07[kg]$ and the mass of the platform is $2.06[kg]$.

3.1. Actuators modeling

The prismatic joints used to drive the mechanism are formed by a linear belt guide Igus® ZLW-1040-02-S-100-L/R-300 with a 300 mm stroke[25], actuated by a Maxon® RE-40 DC motor with a GP42C gearbox with a 15:1 gear ratio[26]. The linear guide is connected to the gearbox with a flexible coupling. A picture of the actuation system is shown in Fig. 5.

As mentioned previously, the dynamics of the actuators is represented by a two degrees of freedom model as in Fig. 2. In equation 20, J_1 is the sum of the inertias of all the components up to the input shaft of the linear ~~drive~~guide. As for the inertia J_2, it is calculated from the mass of the load M_{load} which is formed by the mass of the drive carriage and the inertia of the linear ~~drive~~ guide J_{guide} obtained from the manufacturer. Furthermore the mass M_{load} is translated into a rotational inertia as in equation 21. Finally, J_t is the sum of inertia J_1 and J_2.

$$J_1 = J_{motor} + J_{gearbox} + J_{coupling} \tag{20}$$

$$J_2 = J_{guide} \left(\frac{1}{i_r} \right)^2 + M_{load} \left(\frac{p}{2 \cdot \pi \cdot i_r} \right)^2 \tag{21}$$

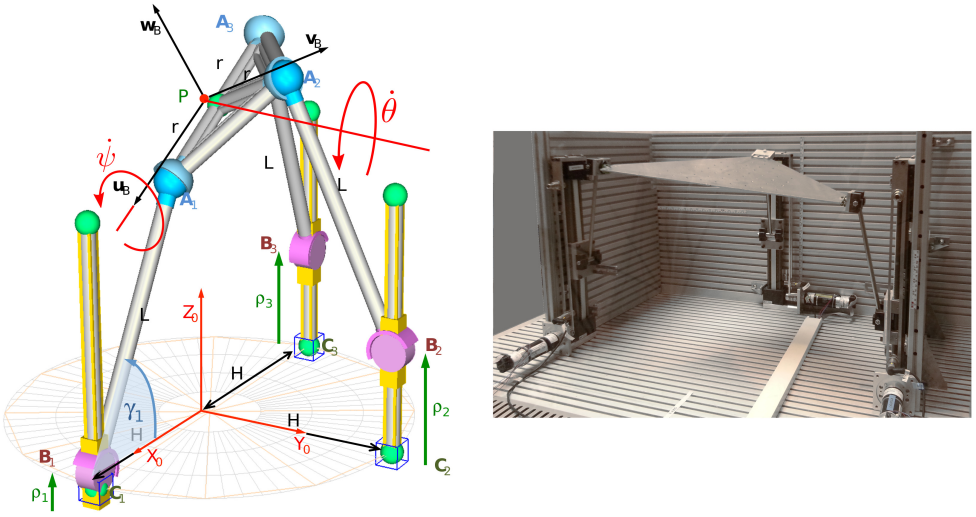

Figure 4: 3PRS PROTOTYPE.

Figure 5: Picture of the actuator.

Where,

$$M_{load} = M_{drive} = 2.27[kg] \tag{22}$$

Also, the linear guides have Coulomb friction τ_f which plays an important role specially at low velocities. This parameter is calculated with equation Eq.23, obtained from the manufacturer's catalogue[25].

$$\tau_f = 0.2 + \left(4.07 \times 10^{-2}\right) M_{load} \tag{23}$$

It is worth mentioning that K_t and C_t in Eqs. 2 and 3 are unknown parameters. Hence, they must be experimentally identified or estimated. To that end, a modal analysis was carried out to obtain the unknown parameters value from the frequency response functions. An accelerometer was placed at the drive carriage and an impact test was performed with a PCB-086-C03 modal hammer. The input signals from the hammer and the vibrations registered by the accelerometer were passed through the OROS-OR35 signal analyzer to obtain the parameters values. Additionally, J_{motor}, $J_{gearbox}$, J_{guide} and $J_{coupling}$ were taken from the manufacturers datasheet[26].

Table 1: Parameter values of the actuator model.

Parameter	Value	Units
f_n *	986.5	$[Hz]$
K_t *	67.702	$[\frac{Nm}{rad}]$
C_t *	3.00×10^{-08}	$[\frac{Nms}{rad}]$
M *	0.076	$[kg]$
J_{motor} **	1.42×10^{-5}	$[kgm^2]$
$J_{gearbox}$ **	1.4×10^{-6}	$[kgm^2]$
$J_{coupling}$ **	4.68×10^{-6}	$[kgm^2]$
J_{guide} **	4.524×10^{-4}	$[kgm^2]$
J_{brake} **	1.00×10^{-6}	$[kgm^2]$

*Experimentally identified

**From manufacturer

3.2. Control and modeling

The control employed in this study is based in a monoarticular local control, where each actuator's position is independently controlled. In this way, the control is performed in the joint space. Moreover, the demanded pose of the mechanism is first passed through the inverse kinematic problem where the joint position are obtained. These are then fed into the joint controller, each one consisting of a cascaded position, velocity and current control. In Fig. 6 a scheme with the actual control implementation is shown.

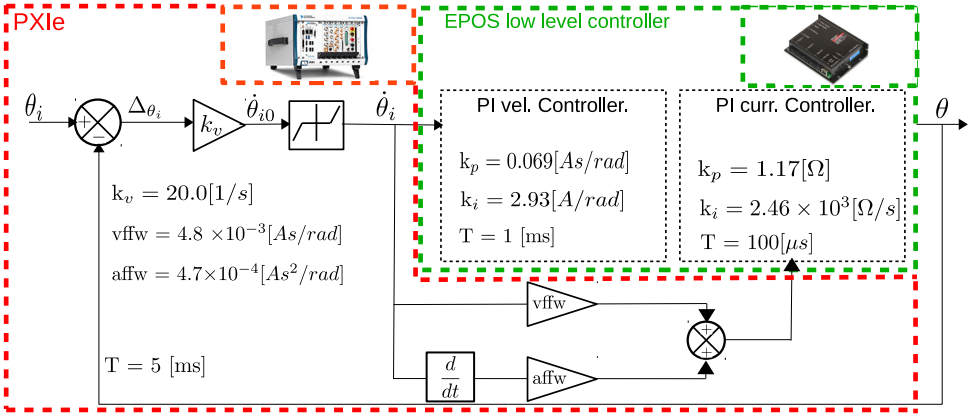

Figure 6: Actual controller.

3.3. Mechanism Dynamics

In this section the dynamics of the MAST prototype are obtained. As for the mechanism bars and the translation dynamics of the platform, the principle of energy equivalence depicted in section 2.4.1 will be followed. On the other hand, the rotation dynamics of the platform will be analyzed using the Boltzmann-Hamel equations as explained in section 2.4.2.

3.3.1. Bars modeling

To model the dynamics of the ~~bars of the mechanism~~ mechanism's bars, the Lagrangian equation ~~of~~for each one is obtained and then the Euler's operator is applied as in equation 4. In this way, equation 24

results, where m_{b_i} and I_{b_i} are the mass and inertia of the i^{th} bar respectively, and g is the gravitational acceleration.

$$\mathbf{f}_{b_i} = \begin{Bmatrix} 0 \\ F_{b_i} \\ 0 \end{Bmatrix} = \mathcal{E}_{\mathbf{q}_{b_i}}(\mathcal{L}_{b_i}) = \begin{bmatrix} m_{b_i} & 0 & 0 \\ 0 & m_{b_i} & 0 \\ 0 & 0 & I_{b_i} \end{bmatrix} \ddot{\mathbf{q}}_{b_i} + \begin{Bmatrix} 0 \\ m_{b_i} g \\ 0 \end{Bmatrix} = \mathbf{M}_{b_i} \ddot{\mathbf{q}}_{b_i} + \mathbf{g}_{b_i} \tag{24}$$

Moreover, by using the kinematic relationship $\dot{\mathbf{q}}_{b_i} = \mathbf{J}_{b_i} \dot{\mathbf{q}}_\rho$ equation 25 is obtained. $\mathbf{J}_{b_i}$ is the Jacobian of each bar which relates the velocity of the center of gravity with the input variables.

$$\mathbf{f}_{b_i} = \mathbf{M}_{b_i} \mathbf{J}_{b_i} \ddot{\mathbf{q}}_\rho + \mathbf{M}_{b_i} \dot{\mathbf{J}}_{b_i} \dot{\mathbf{q}}_\rho + \mathbf{g}_{b_i} \tag{25}$$

The expression of the $\mathbf{J}_{b_i}$ is shown in the appendix. What is more, the contribution of each leg i to the overall mechanism's dynamics $\mathbf{f}_{\rho_{b_i}}$ is found by employing equation 7, thus obtaining~~:~~ the expression in Eq. 26.

$$\mathbf{f}_{\rho_{b_i}} = \mathbf{J}_{b_i}^T \mathbf{f}_{b_i} = \left[\mathbf{J}_{b_i}^T \mathbf{M}_{b_i} \mathbf{J}_{b_i}\right] \ddot{\mathbf{q}}_\rho + \left[\mathbf{J}_{b_i}^T \mathbf{M}_{b_i} \dot{\mathbf{J}}_{b_i} \dot{\mathbf{q}}_\rho\right] + \left[\mathbf{J}_{b_i}^T \mathbf{g}_{b_i}\right] \tag{26}$$

~~Equation 26~~ Furthermore, Eq. 26 can be simplified by operating the matrices and renaming them afterwards. In this way, equation 27 results.

$$\mathbf{f}_{\rho_{b_i}} = \mathbf{I}_{b_i} \ddot{\mathbf{q}}_\rho + \mathbf{c}_{b_i} + \bar{\mathbf{g}}_{b_i} \tag{27}$$

Where $\mathbf{I}_{b_i}$ and $\bar{\mathbf{g}}_{b_i}$ are the inertia matrix and gravitational vector respectively. These are only functions of the position of the mechanism. On the other hand, $\mathbf{c}_{b_i}$ is the matrix containing velocity quadratic terms.

3.3.2. Modeling of the end-effector

As mentioned before, the MAST mechanism is capable of constrained translation and rotation motions. The translation dynamics has been analyzed as described in section 2.4.2 and following equations 8 and 9. On the other hand, the rotation dynamics is analyzed by considering a virtual inertial body and applying Boltzmann-Hamel equations. A moving coordinate system is placed at the point P as shown in Fig. 4. Furthermore, the angular velocity $\mathbf{w}$ in the moving frame is used as *quasi-velocities* for the application of the Boltzmann-Hamel equations. Since only the rotation motion of the platform is being analyzed, the translation and potential energies are neglected. Hence, the Lagrangian function of the moving platform results in:

$$\mathcal{L}_{mp} = \overline{\mathbf{T}} = \frac{1}{2} \mathbf{w}^T \mathbf{I}_{mp} \mathbf{w} \tag{28}$$

Where $\mathbf{w}$ is the angular velocity,

$$\mathbf{w} = [\omega_x, \omega_y, \omega_x]^T \tag{29}$$

and $\mathbf{I}_{mp}$ is the inertia tensor of the platform in the local reference system. Also, the assembled condition of the platform with the rest of the mechanism is provided by the loop-closure and constrained equations. These relate the angular velocity $\mathbf{w}$ with the input variables velocities in $\dot{\mathbf{q}}_\rho$ as follows.

$$\mathbf{w} = \mathbf{J}_R \dot{\mathbf{q}}_\rho \tag{30}$$

Where the expression of $\mathbf{J}_R$ is shown in the appendix. Moreover, by substituting Eq. 12 into Eq. 30, the relationship between the Euler angles and the inputs can be found.

$$\dot{\mathbf{q}}_e = \left(\mathbf{D}_\phi{}^T\right)^{-1} \mathbf{J}_R \dot{\mathbf{q}}_\rho = \mathbf{J} \dot{\mathbf{q}}_\rho \tag{31}$$

By following the procedure depicted in section 2.4.2, and recalling equations 18 and 19, the expression of the rotation dynamics is obtained.

$$\mathbf{J}_R^T \mathbf{m}_{mp} = \mathbf{J}_R^T \mathbf{I}_{mp} \mathbf{J}_R \ddot{\mathbf{q}}_\rho + \mathbf{c}_{mp} = \bar{\mathbf{I}}_{mp} \ddot{\mathbf{q}}_\rho + \mathbf{c}_{mp}$$

Where,

$$\mathbf{c}_{mp} = \left[\mathbf{J}^T \left[\mathbf{D}_\phi \mathbf{I}_{mp} \mathbf{D}_\phi{}^T\right] \dot{\mathbf{J}} + \mathbf{J}^T \left[\mathbf{D}_\phi \mathbf{I}_{mp} \dot{\mathbf{D}}_\phi^T + 2\dot{\mathbf{D}}_\phi \mathbf{I}_{mp} \mathbf{D}_\phi{}^T - \mathbf{A}^T \mathbf{I}_{mp} \mathbf{D}_\phi{}^T\right] \mathbf{J}\right] \dot{\mathbf{q}}_\rho$$

3.3.3. Global dynamics

Finally, the explicit dynamic equations of the 3PRS is obtained by adding the dynamic contribution of the legs (Eq. 27), and the translational and rotational dynamic contributions of the platform (equations 9 and 18 respectively).In this way, Eq. 32 is obtained where $\mathbf{I}_{Ls}$, $\mathbf{c}_{Ls}$ and $\mathbf{g}_{Ls}$ are the inertial, Coriolis and gravitational terms of the bars. Similarly, it is recalled that $\mathbf{I}_G$ and $\mathbf{c}_G$ represent the inertial and Coriolis terms for the translational dynamics whereas $\bar{\mathbf{I}}_{mp}$ and $\mathbf{c}_{mp}$ represent the dynamics due to the rotation.

$$\mathbf{t}_\rho + \mathbf{J}_G^T \mathbf{f}_G + \mathbf{J}_R^T \mathbf{m}_{mp} = \left[\mathbf{I}_{Ls} + \mathbf{I}_G + \bar{\mathbf{I}}_{mp}\right] \ddot{\mathbf{q}}_\rho + \left[\mathbf{c}_{Ls} + \mathbf{c}_G + \mathbf{c}_{mp}\right] + \left[\bar{\mathbf{g}}_{Ls} + \bar{\mathbf{g}}_G\right] \tag{32}$$

It can be seen that with the approach followed, the Jacobians $\mathbf{J}_{bi}$, $\mathbf{J}_G$ and $\mathbf{J}_R$ are obtained from the kinematic analysis in a straightforward way after applying the loop-closure and constrained equations. Furthermore, matrices $\mathbf{D}_\phi{}^T$ and $\mathbf{A}$ can be defined for an Euler convention, hence, not depending on any specific mechanism.

4. Experimental validation

To validate the model of the system, the frequency response was analyzed and the bandwidth of the simulation model was compared with the experimental results obtained from the prototype.~~Finally~~ Also, the modeled and measured torque outputs were compared. As a result, the interaction of the mechanism's and actuators's models can be easily studied and compared with experimental data.

4.1. Frequency domain testing

In Fig. 7 a bode diagram is shown with the magnitude and phase response of the transfer functions in equations 2 and 3 using the values of Table 1. It can be seen that the resonant frequency of the TF_2 is located at 900 [Hz] approximately, which is significantly higher that the intended operating frequency range of the system.

Also, for a MAST mechanism it is important to study the bandwidth of the system to know up to which frequency could be simulated. For this reason, pure sinusoidal motions in z, ψ and θ were simulated in the 0.5-20[Hz] frequency range using the mechatronic model. For the experimental tests, the same motions have been commanded with frequencies set to 0.4, 1, 5 10 and 20 [Hz]. A comparison between the simulation and the experimental tests is shown in Figs.8 and 9. ~~Moreover, the same frequencies were executed without the mechanism in order to study the influence of the MAST on the actuation system's bandwidth (Fig.10)~~ Moreover, to study the interaction between the actuation system and the mechanism, the bandwidth with and without the mechanism is compared in Fig. 10

From figures 8 and 9 it can be seen that the simulations are in close correspondence with the experimental results obtained for each motion. Furthermore, when the two motions are compared, no significant differences are present in the system's performance despite the fact that both motions are different. This leads to the idea that the mechanism does not exerts a significant influence on the system's performance. This can be further analyzed with the z motion in Fig. 10.

~~It is appreciated how the simulation is similar to the behavior observed with the experimental tests. On the other hand, the simulation shows that the actuators without the mechanism attached have a bandwidth about 4[Hz]. However when the mechanism is present, the system's bandwidth is reduced to 3.5 [Hz] for all the motions tested.~~

As mentioned before, in Fig. 10 the response magnitude and phase for the z motion is shown. What is more, the same motion is compared with the MAST attached and with only the actuators. In this way,

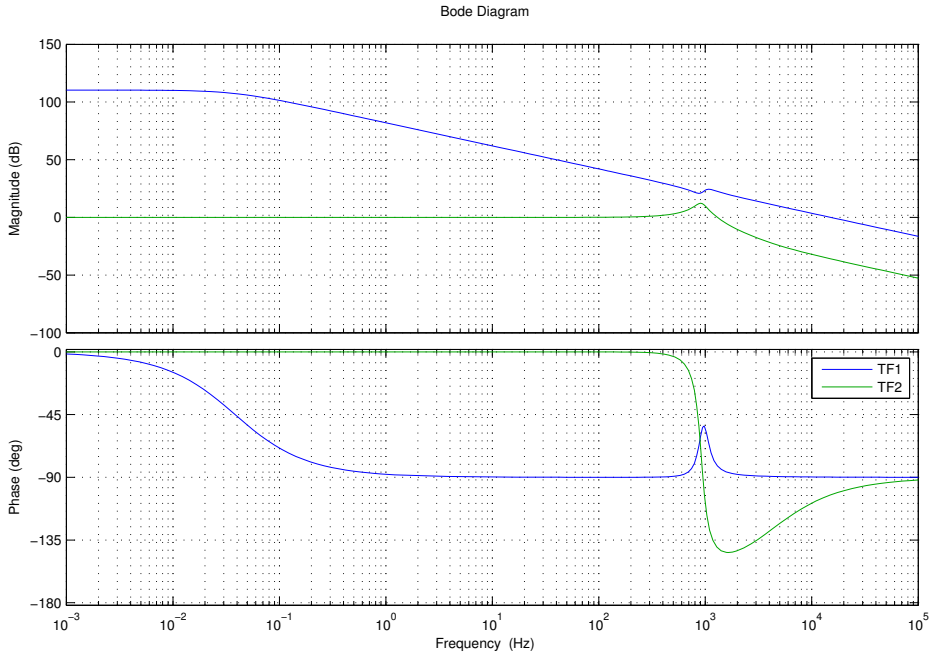

Figure 7: Bode plot of the two transfer functions of the actuators.

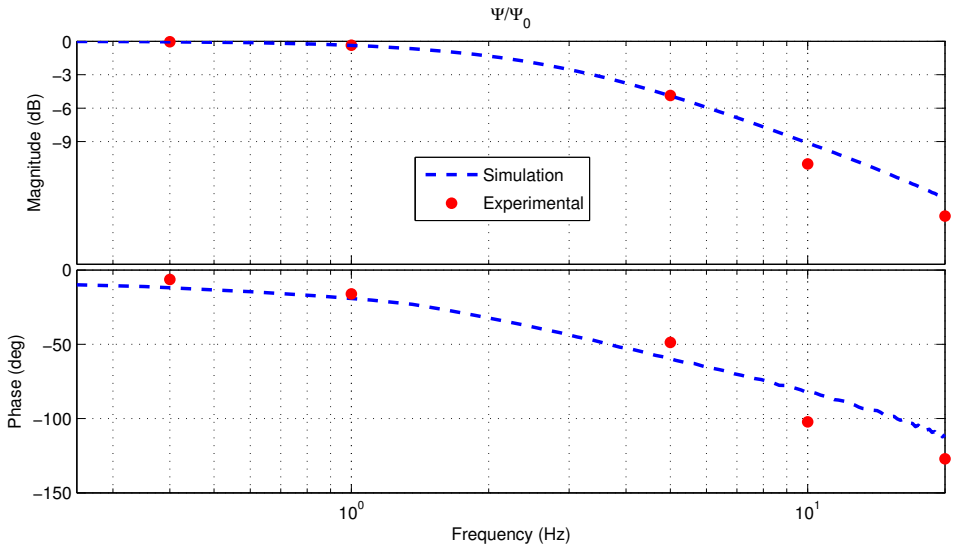

Figure 8: Manipulator closed position loop transfer function for the ψ motion.

it can be easily analyzed the effect of the mechanism in the system's response. It is appreciated that up to 2[Hz] both systems behave similarly. However at 2 [Hz] the magnitude of their response start diverging.

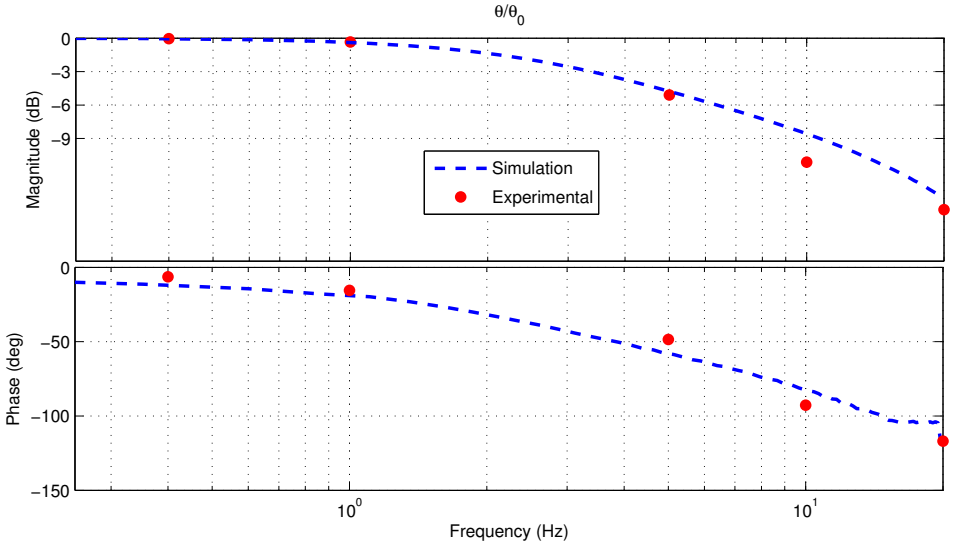

Figure 9: Manipulator closed position loop transfer function for the θ motion.

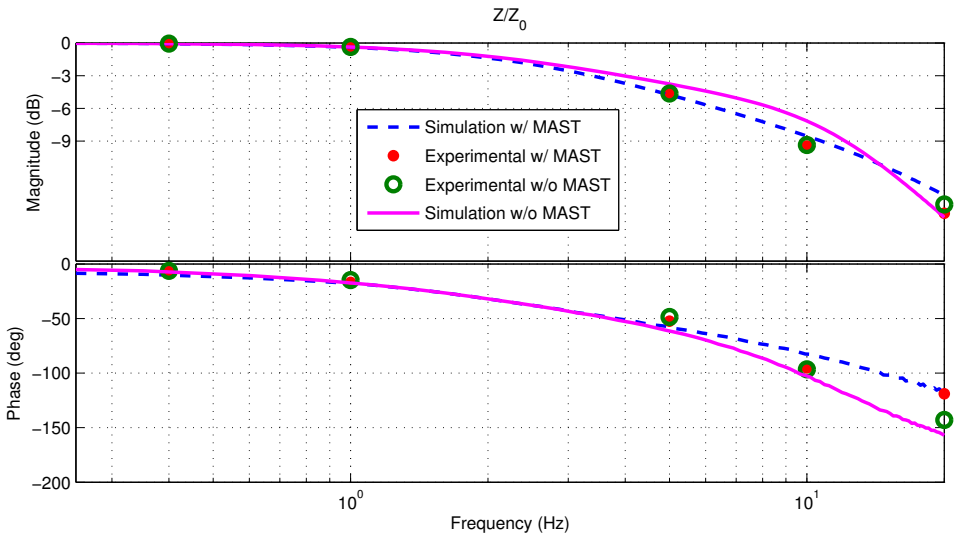

Figure 10: Manipulator closed position loop transfer function for the actuator model with and without the MAST attached.

What is more, it has been found that the actuators without the MAST have a bandwidth about 4[Hz], whereas with the mechanism the bandwidth is reduced to 3.5[Hz]. Thus, it can be noted that the actuators are the most limiting components and that the mechanism itself has only a 0.5[Hz] effect on the system's performance.

4.2. Time domain tests

Finally, in Figs.11-13 the position and the torques are shown for the three pure motions executed at frequencies 0.4, 5 and 10 [Hz]. Two set of model parameters were used to simulated the model and compare the results with the measurements. The simulation with the parameter set *Sim. Manufac.* was constructed with the data as obtained from the manufacturers, whereas the simulation *Sim. Ident.* was constructed by modifying the inertia $J1$ to $J1/1.56$ and the Coulomb friction modified to $7.18 \times 10^{-2}[Nm]$ as it will be explained in the next paragraph.

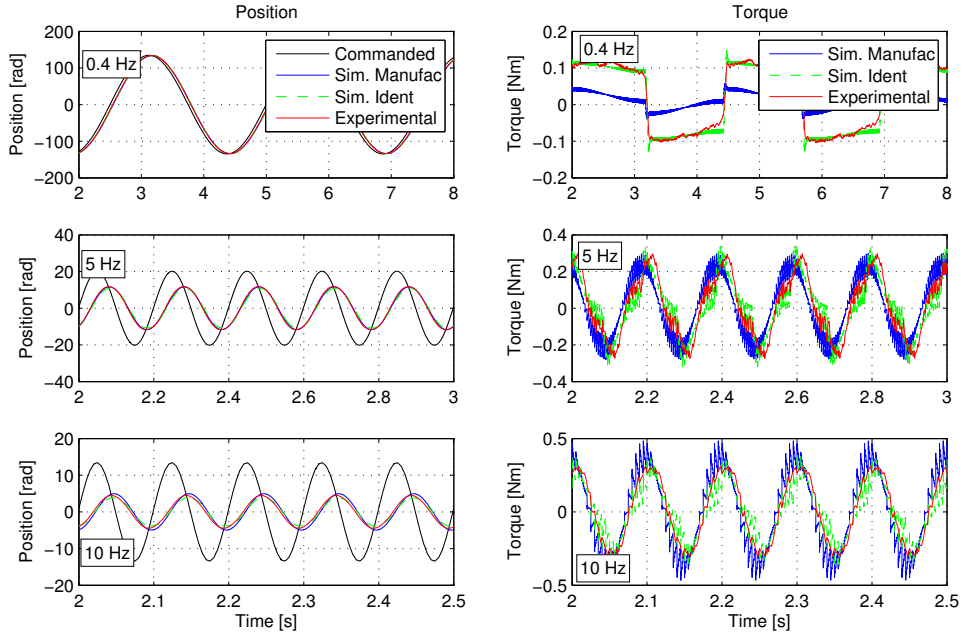

Figure 11: Position and torque signals comparison for the z motion.

From the figures, the simulated positions present and maximum deviation of approximately 11% in magnitude and 13% in phase respect to the experimental signals for the frequencies shown and motions executed. Also, it can be observed that as the frequencies of the motions are increased, the magnitude of the response is reduced in accordance with the Bodes shown previously. Indeed, at 0.4[Hz] the magnitude of the response was found to be approximately 99.4%, whereas at 5 [Hz] and 10 [Hz] the obtained magnitudes were 65.4% and 43.2% respectively. Likewise, the phase lag between the commands and the actual signals are appropriately estimated by the model when compared with the experimental data. It can be seen that at 0.4 [Hz], 5 [Hz] and 10 [Hz], the phase lags were found to be $-6.3°$, $-62.5°$ and $-103.7°$ respectively.

Nevertheless and to validate the model, the position response must not be used alone as the controller's action may be masquerading dynamic deviations with the appearance of good positioning results. This effect can be clearly seen by comparing the position and the torque of the *Sim. Manufac.* model at 0.4 [Hz]. It is observed that, despite an apparent good positioning with respect to the experimental data, the simulated torque differs from the experimental torque obtained by approximately 70%. This indicates that the dynamics are not correctly represented by this model.

Moreover ~~. On the other hand,~~the torques obtained from the simulation with the two parameters set are different. When the data as given by the manufacturer was introduced, a difference in the torque of approximately 0.10[Nm] at 0.4[Hz] can be appreciated as it was pointed out before. This implies that the Coulomb friction force in the actual system is higher. Also, at a frequency of 10[Hz], the model estimated 0.1[Nm] higher torque than the experimental signals. Since the acceleration forces increase with the frequencies, it

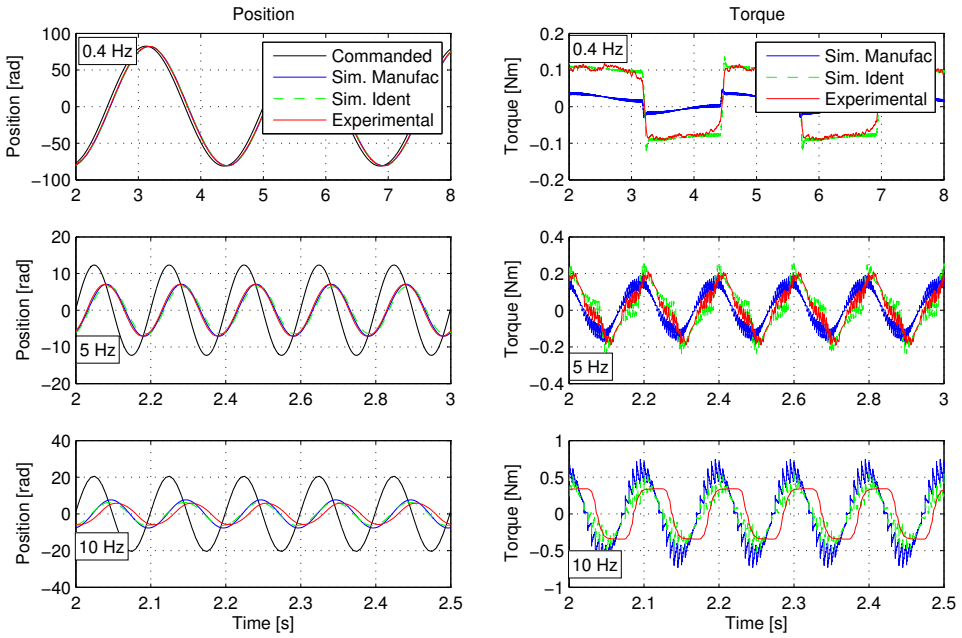

Figure 12: Position and torque signals comparison for the ψ motion.

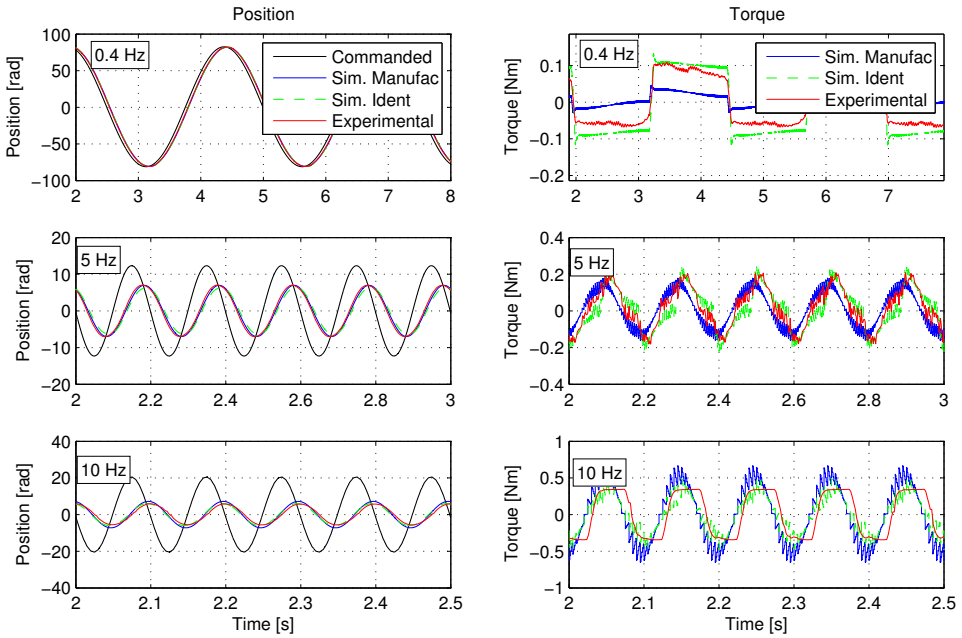

Figure 13: Position and torque signals comparison for the θ motion.

follows that the actual inertia should be less than the initially estimated with the manufacturer data. For this reason, the Coulomb friction and the inertia J_1 were adjusted as ~~mentioned~~commented before. In this way, the simulation provided better results than when the parameters set with the original manufacturer

data was used.

On top of that, it is worth observing that even when the inputs are pure sinusoids, the resulted torques are not sinusoids as well. This effect is caused by the non-linearities of the dynamics and the friction present in the actuation system. The latter can be easily identified at lower frequencies, specially at 0.4 [Hz] where an almost square signal is appreciated. Finally, it can also be seen that at 10 [Hz] the experimental torque are *trimmed* by the action of a low-pass filter attributed to the low level controller.

5. Conclusions

In the present work a mechatronic model has been developed for a 3PRS parallel manipulator. A key contribution of this work is that the mechanism dynamics is integrated as a disturbance applied to the actuators. This results in a simple yet reliable model that integrates the actuators dynamics with the manipulator model in a decoupled manner. In this way, different configurations or design of individual components can be easily modified and then integrated to evaluate the overall system's performance without compromising reliability of the results.

Furthermore, the manipulator's dynamics was described using Boltzmann-Hamel equations and the principle of energy equivalence as shown is section 3.3. It was found that, since the translation and rotation motions are decoupled, the main advantage of Boltzmann-Hamel equations becomes apparent when applied to analyze the rotation dynamics. Furthermore, the approach taken simplifies obtaining explicit dynamic equations, where complex and nonlinear expressions are avoided by making use of the kinematic Jacobians. As a contribution, the proposed procedure has the advantage of being systematic, which is less error prone than when trying to obtain particular dynamic equations for a given mechanism.

Also, the actuators and the control scheme have been modeled. They were further integrated into the mechatronic model and its performance was compared with an actual prototype of a MAST. It was observed that the mechatronic model resulted in an useful simulation tool to assess the performance of the system in terms of bandwidth.

Moreover, when the simulations and experimental signals where compared, it was observed a reasonably agreement. The motor positions of both signals present the same amplitude and the phase lag shows a slight difference attributed to the friction and other phenomena yet to be explored. Also, it was observed that with the parameters values obtained from the manufacturer, the model provided fairly good results. However, with the Coulomb friction and inertia adjusted, the model provided more accurate results. This shows that an identification step should be taken in order to take into account differences between the theoretic and actual values for the parameters.

References

[1] Physik Instrumente (PI) GmbH & Co. KG, URL `http://www.physikinstrumente.com/products/parallel-kinematic-hexapods.html`, last visited on October 14th, 2015.

[2] PKMtricept SL, URL `http://www.pkmtricept.com/`, last visited on October 15th, 2015.

[3] Adept Technology, Inc., URL `http://www.adept.com/products/robots`, last visited on October 14th, 2015.

[4] Moog Inc, URL `http://www.moog.com/products/hexapods-positioning-systems/`, last visited on October 15th, 2015.

[5] L. Žlajpah, Simulation in robotics, Mathematics and Computers in Simulation 79 (4) (2008) 879 – 897, ISSN 0378-4754, URL `http://www.sciencedirect.com/science/article/pii/S0378475408001183`, 5th Vienna International Conference on Mathematical Modelling/Workshop on Scientific Computing in Electronic Engineering of the 2006 International Conference on Computational Science/Structural Dynamical Systems: Computational Aspects.

[6] B. Siciliano, L. Sciavicco, L. Villani, G. Oriolo, Robotic: Modelling, Planning and Control, Advanced Textbooks in Control and Signal Processing, Springer-Verlag London Limited, 2010.

[7] J. Wang, C. Gosselin, L. Cheng, Modeling and Simulation of Robotic Systems with Closed Kinematic Chains Using the Virtual Spring Approach, Multibody System Dynamics 7 (2) (2002) 145–170, ISSN 1384-5640.

[8] M. P. Massimo Callegari, Matteo-Claudio Palpacelli, Dynamics modelling and cotrol of the 3-RCC translational platform, Mechatronics (16) (2006) 589–605.

[9] Y. Lou, Z. Li, Y. Zhong, J. Li, Z. Li, Dynamics and contouring control of a 3-DoF parallel kinematics machine, Mechatronics 21 (1) (2011) 215 – 226, ISSN 0957-4158.

[10] A. Codourey, Dynamic Modeling of Parallel Robots for Computed-Torque Control Implementation, The International Journal of Robotics Research 17 (12) (1998) 1325–1336.

[11] C. Yang, Q. Huang, J. Han, Computed force and velocity control for spatial multi-DOF electro-hydraulic parallel manipulator, Mechatronics 22 (6) (2012) 715 – 722, ISSN 0957-4158, special Issue on Intelligent Mechatronics (LSMS2010 & ICSEE2010).
[12] I. Ebert-Uphoff, C. Gosselin, Dynamic modeling of a class of spatial statically-balanced parallel platform mechanisms, in: Robotics and Automation, 1999. Proceedings. 1999 IEEE International Conference on, vol. 2, ISSN 1050-4729, 881–888 vol.2, 1999.
[13] R. Oftadeh, M. Aref, H. Taghirad, Explicit dynamics formulation of Stewart-Gough platform: A Newton-Euler approach, in: Intelligent Robots and Systems (IROS), 2010 IEEE/RSJ International Conference on, ISSN 2153-0858, 2772–2777, 2010.
[14] M. Callegari, M.-C. Palpacelli, M. Principi, Dynamics modelling and control of the 3-RCC translational platform, Mechatronics 16 (10) (2006) 589 – 605, ISSN 0957-4158, URL http://www.sciencedirect.com/science/article/pii/S0957415806000754.
[15] H. Abdellatif, B. Heimann, Computational efficient inverse dynamics of 6-DOF fully parallel manipulators by using the Lagrangian formalism, Mechanism and Machine Theory 44 (1) (2009) 192 – 207, ISSN 0094-114X, URL http://www.sciencedirect.com/science/article/pii/S0094114X08000311.
[16] K. Ebert-Uphoff, I; Kozak, Review of the Role of Quasi-Coordinates for the Kinematic and Dynamic Modeling of Parallel Manipulators., in: Proceedings of the Workshop on Fundamental Issues and Future Research Directions for Parallel Mechanisms and Manipulators, Quebec, 328–338, 2002.
[17] A. Lurie, Analytical Mechanics, Foundations of Engineering Mechanics, Springer Berlin Heidelberg, ISBN 978-3-642-53650-2, 2002.
[18] G. Magnani, P. Rocco, Mechatronic analysis of a complex transmission chain for performance optimization in a machine tool, Mechatronics 20 (1) (2010) 85 – 101, ISSN 0957-4158, special Issue on Servo Control for Data Storage and Precision Systems, from 17th {IFAC} World Congress 2008.
[19] G. Ellis, Control System Design Guide (Third Edition), Academic Press, Burlington, third edition edn., ISBN 978-0-12-237461-6, URL http://www.sciencedirect.com/science/article/pii/B9780122374616500126, 2004.
[20] H. Groß, J. Hamann, G. Wiegärtner, Electrical Feed Drives in Automation: Basics, Computation, Dimensioning, Publicis MCD Corporate Publishing, Erlangen and Munich, 2001.
[21] F. Paccot, N. Andreff, P. Martinet, A Review on the Dynamic Control of Parallel Kinematic Machines: Theory and Experiments, The International Journal of Robotics Research 28 (3) (2009) 395–416, URL http://ijr.sagepub.com/content/28/3/395.abstract.
[22] S. Flottmeier, A. Trchtler, 2-DOF state control scheme for the motion control of a parallel kinematic machine, in: 2013 Conference on Control and Fault-Tolerant Systems (SysTol), ISSN 2162-1195, 744–749, 2013.
[23] H. Pang, M. Shahinpoor, Inverse dynamics of a parallel manipulator, Journal of Robotic Systems 11 (8) (1994) 693–702, ISSN 1097-4563, URL http://dx.doi.org/10.1002/rob.4620110803.
[24] M.-S. Tsai, W.-H. Yuan, Inverse dynamics analysis for a 3-PRS parallel mechanism based on a special decomposition of the reaction forces, Mechanism and Machine Theory 45 (11) (2010) 1491 – 1508, ISSN 0094-114X, URL http://www.sciencedirect.com/science/article/pii/S0094114X10001229.
[25] Igus-GmbH, Drylin ZLW -1040 Toothed belt axis online catalog, URL http://www.igus.eu/wpck/4773/zlw_1040, 2016.
[26] Maxon, Maxon motor online catalog, URL http://www.maxonmotor.com/maxon/view/catalog/, 2016.
[27] J. Carretero, R. Podhorodeski, M. Nahon, C. Gosselin, Kinematic Analysis and Optimization of a New Three Degree-of-Freedom Spatial Parallel Manipulator., ASME. J. Mech. Des. 122 (1) (1999) 17–24.

Acknowledgment

The authors of this paper wish to acknowledge the funding received from the Spanish Government via the Ministerio de Economía y Competitividad (BES-2012-053723 under Project DPI2011-22955 and DPI2015-64450-R), the ERDF of the European Union, the Government of the Basque Country (SAIOTEK 2013 SAI13/245), and the financial support from the University of the Basque Country(UPV/EHU) under the program UFI 11/29.

Appendix A. Jacobian matrices

From the kinematic analysis of the manipulator[27] the following linear system results.

$$\begin{bmatrix} \\ J_x \\ \\ \end{bmatrix} \begin{Bmatrix} \dot{z}_p \\ \dot{\psi} \\ \dot{\theta} \end{Bmatrix} = \begin{bmatrix} \\ J_q \\ \\ \end{bmatrix} \begin{Bmatrix} \dot{\rho}_1 \\ \dot{\rho}_2 \\ \dot{\rho}_3 \end{Bmatrix} \tag{A.1}$$

Where,

$$J_{x_{11}} = Lsin(\gamma_1) \tag{A.2}$$
$$J_{x_{12}} = Lrsin(\theta)cos(\psi)cos(\gamma_1) \tag{A.3}$$
$$J_{x_{13}} = Lrcos(\theta)sin(\psi)cos(\gamma_1) + Lrsin(\theta - \gamma_1) \tag{A.4}$$
$$J_{x_{21}} = Lsin(\gamma_2) \tag{A.5}$$
$$J_{x_{22}} = Lr(sin(\psi)cos(\gamma_2) + cos(\theta)cos(\psi)sin(\gamma_2)) \tag{A.6}$$
$$J_{x_{23}} = Lrsin(\theta)sin(\psi)sin(\gamma_1) \tag{A.7}$$
$$J_{x_{31}} = Lsin(\gamma_3) \tag{A.8}$$
$$J_{x_{32}} = -Lrsin(\theta)cos(\psi)cos(\gamma_3) \tag{A.9}$$
$$J_{x_{32}} = -Lrcos(\theta)sin(\psi)cos(\gamma_3) + Lrsin(\theta + \gamma_3) \tag{A.10}$$

And,

$$J_q = \begin{bmatrix} Lsin(\gamma_1) & 0 & 0 \\ 0 & Lsin(\gamma_2) & 0 \\ 0 & 0 & Lsin(\gamma_3) \end{bmatrix} \tag{A.11}$$

Also, the TCP (point p) of the manipulator can only move in the x and z directions. Hence, the following relations can be found.

From bar 1:

$$\dot{x}_p = L\dot{\gamma_1}sin(\gamma_1) + r\dot{\theta}sin(\theta) \tag{A.12}$$
$$\dot{z}_p = \dot{\rho_1} + L\dot{\gamma_1}cos(\gamma_1) + r\dot{\theta}cos(\theta) \tag{A.13}$$

From bar 2:

$$-r\dot{\psi}sin(\psi) = L\dot{\gamma_2}sin(\gamma_2) \tag{A.14}$$
$$\dot{z}_p = \dot{\rho_2} + L\dot{\gamma_2}cos(\gamma_2) + r\dot{\theta}sin(\theta)sin(\psi) - r\dot{\theta}cos(\theta)cos(\psi) \tag{A.15}$$

From bar 3:

$$\dot{x}_p = -L\dot{\gamma_3}sin(\gamma_3) - r\dot{\theta}sin(\theta) \tag{A.16}$$
$$\dot{z}_p = \dot{\rho_3} + L\dot{\gamma_3}cos(\gamma_3) - r\dot{\theta}cos(\theta) \tag{A.17}$$

Moreover, the velocities of the center of mass for each bar can be calculated from the velocities of point p. In the following, the expressions for the bar 1 will be obtained.

$$\dot{x}_1 = \frac{1}{2}\left(\dot{x}_p - r\dot{\theta}sin(\theta)\right) \tag{A.18}$$
$$\dot{z}_1 = \frac{1}{2}\dot{\rho}_1 + \frac{1}{2}\left(\dot{z}_p - r\dot{\theta}cos(\theta)\right) \tag{A.19}$$
$$\dot{\gamma_1} = \frac{1}{Lsin(\gamma_1)}\left(\dot{x}_p - r\dot{\theta}sin(\theta)\right) \tag{A.20}$$
$$\tag{A.21}$$

Substituting the $\dot{x}_p$ and $\dot{z}_p$ by expressions A.12 and A.13 respectively, the following expression results.

$$\begin{Bmatrix} \dot{x}_1 \\ \dot{z}_1 \\ \dot{\gamma}_1 \end{Bmatrix} = \begin{bmatrix} 0 & -\frac{1}{2}rsin(\theta)cos(\psi) & -\frac{1}{2}\left(rsin(\theta)+rcos(\theta)sin(\psi)\right) \\ \frac{1}{2} & 0 & -\frac{1}{2}rcos(\theta) \\ 0 & -\frac{rsin(\theta)cos(\psi)}{Lsin(\gamma_1)} & -\frac{rsin(\theta)+rcos(\theta)sin(\psi)}{Lsin(\gamma_1)} \end{bmatrix} \begin{Bmatrix} \dot{z}_p \\ \dot{\psi} \\ \dot{\theta} \end{Bmatrix} + \begin{Bmatrix} 0 \\ \frac{\dot{\rho}_1}{2} \\ 0 \end{Bmatrix} \tag{A.22}$$

The above expression can be rewritten as a function of the inputs as follows.

$$\begin{Bmatrix} \dot{x}_1 \\ \dot{z}_1 \\ \dot{\gamma}_1 \end{Bmatrix} = \begin{bmatrix} 0 & -\frac{1}{2}rsin(\theta)cos(\psi) & -\frac{1}{2}\left(rsin(\theta)+rcos(\theta)sin(\psi)\right) \\ \frac{1}{2} & 0 & -\frac{1}{2}rcos(\theta) \\ 0 & -\frac{rsin(\theta)cos(\psi)}{Lsin(\gamma_1)} & -\frac{rsin(\theta)+rcos(\theta)sin(\psi)}{Lsin(\gamma_1)} \end{bmatrix} \begin{bmatrix} \\ J_x^{-1}J_q \\ \\ \end{bmatrix} \begin{Bmatrix} \dot{\rho}_1 \\ \dot{\rho}_2 \\ \dot{\rho}_3 \end{Bmatrix} + \begin{Bmatrix} 0 \\ \frac{\dot{\rho}_1}{2} \\ 0 \end{Bmatrix} \tag{A.23}$$

Finally, the Jacobian matrix for the bar 1 results in:

$$J_{b_1} = \begin{bmatrix} 0 & -\frac{1}{2}rsin(\theta)cos(\psi) & -\frac{1}{2}\left(rsin(\theta)+rcos(\theta)sin(\psi)\right) \\ \frac{1}{2} & 0 & -\frac{1}{2}rcos(\theta) \\ 0 & -\frac{rsin(\theta)cos(\psi)}{Lsin(\gamma_1)} & -\frac{rsin(\theta)+rcos(\theta)sin(\psi)}{Lsin(\gamma_1)} \end{bmatrix} \begin{bmatrix} \\ J_x^{-1}J_q \\ \\ \end{bmatrix} + \begin{bmatrix} 0 & 0 & 0 \\ \frac{1}{2} & 0 & 0 \\ 0 & 0 & 0 \end{bmatrix} \tag{A.24}$$

With the linear system being

$$\begin{Bmatrix} \dot{x}_1 \\ \dot{z}_1 \\ \dot{\gamma}_1 \end{Bmatrix} = \begin{bmatrix} \\ J_{b_1} \\ \\ \end{bmatrix} \begin{Bmatrix} \dot{\rho}_1 \\ \dot{\rho}_2 \\ \dot{\rho}_3 \end{Bmatrix} \tag{A.25}$$

By following a similar procedure for bars 1 and 2, the linear systems and their respective Jacobians are obtained.

$$\begin{Bmatrix} \dot{y}_2 \\ \dot{z}_2 \\ \dot{\gamma}_2 \end{Bmatrix} = \begin{bmatrix} \\ J_{b_2} \\ \\ \end{bmatrix} \begin{Bmatrix} \dot{\rho}_1 \\ \dot{\rho}_2 \\ \dot{\rho}_3 \end{Bmatrix} \tag{A.26}$$

$$\begin{Bmatrix} \dot{x}_3 \\ \dot{z}_3 \\ \dot{\gamma}_3 \end{Bmatrix} = \begin{bmatrix} \\ J_{b_3} \\ \\ \end{bmatrix} \begin{Bmatrix} \dot{\rho}_1 \\ \dot{\rho}_2 \\ \dot{\rho}_3 \end{Bmatrix} \tag{A.27}$$

With,

$$J_{b_2} = \begin{bmatrix} 0 & -\frac{1}{2}rsin(\psi) & 0 \\ 0 & -\frac{cos(\gamma_2)}{2sin(\gamma_2)}rsin(\psi) & 0 \\ 0 & -\frac{rsin(\psi)}{Lsin(\gamma_2)} & 0 \end{bmatrix} \begin{bmatrix} \\ J_x^{-1}J_q \\ \\ \end{bmatrix} + \begin{bmatrix} 0 & 0 & 0 \\ 0 & 1 & 0 \\ 0 & 0 & 0 \end{bmatrix} \tag{A.28}$$

$$J_{b_3} = \begin{bmatrix} 0 & -\frac{1}{2}rsin(\theta)cos(\psi) & -\frac{1}{2}\left(rsin(\theta)-rcos(\theta)sin(\psi)\right) \\ \frac{1}{2} & 0 & \frac{1}{2}rcos(\theta) \\ 0 & \frac{rsin(\theta)cos(\psi)}{Lsin(\gamma_3)} & -\frac{rsin(\theta)+rcos(\theta)sin(\psi)}{Lsin(\gamma_3)} \end{bmatrix} \begin{bmatrix} \\ J_x^{-1}J_q \\ \\ \end{bmatrix} + \begin{bmatrix} 0 & 0 & 0 \\ 0 & 0 & \frac{1}{2} \\ 0 & 0 & 0 \end{bmatrix} \tag{A.29}$$

As for the rotation Jacobian of the end effector, the following linear system relates the angular velocities of point p with the angular velocities $\dot{\psi}$ and $\dot{\theta}$.

$$\begin{Bmatrix} w_x \\ w_y \\ w_z \end{Bmatrix} = \begin{bmatrix} 1 & 0 \\ 0 & cos(\psi) \\ 0 & -sin(\psi) \end{bmatrix} \begin{Bmatrix} \dot{\psi} \\ \dot{\theta} \end{Bmatrix} \tag{A.30}$$

Moreover, the equation can be expressed as a function of the inputs as follows.

$$\begin{Bmatrix} w_x \\ w_y \\ w_z \end{Bmatrix} = \begin{bmatrix} 1 & 0 \\ 0 & cos(\psi) \\ 0 & -sin(\psi) \end{bmatrix} \begin{bmatrix} \\ J_x^{-1}J_q|_R \\ \\ \end{bmatrix} \begin{Bmatrix} \dot{\rho}_1 \\ \dot{\rho}_2 \\ \dot{\rho}_3 \end{Bmatrix} \tag{A.31}$$

Where $J_x^{-1}J_q|_R$ is the submatrix of $J_x^{-1}J_q$ from row 2 and 3, which is the matrix that relates the rotation motion of point p with the inputs. Hence, the Jacobian matrix of the end effector results in.

$$J_R = \begin{bmatrix} 1 & 0 \\ 0 & cos(\psi) \\ 0 & -sin(\psi) \end{bmatrix} \begin{bmatrix} \\ J_x^{-1}J_q|_R \\ \\ \end{bmatrix} \tag{A.32}$$